Coherent excitations at the neutral-ionic transition: Femtosecond dynamics on diabatic potential energy surfaces

Lorenzo Cavatorta and Anna Painelli*
Dipartimento di Chimica, Universitá di Parma, 43100 Parma, Italy

Zoltán G. Soos
Department of Chemistry, Princeton University, Princeton, New Jersey 08540, USA
(Received 19 February 2015; revised manuscript received 16 April 2015; published 1 May 2015)

Upon decreasing temperature ($T_c \sim 81$ K) tetrathiafulvalene-chloranil (TTF-CA) undergoes a discontinuous phase transition from a neutral regular stack to an ionic dimerized stack. The same system may undergo a phase transition upon photoexcitation. We discuss the early time (<3 ps) dynamics following ultrafast (<20 fs) excitation of TTF-CA crystals either near or far from the neutral-ionic transition ($T \sim 90$ and 260 K, respectively). Adopting a modified Hubbard model with linear coupling of electrons to a zone-center lattice (dimerization) phonon and to a molecular vibration, both assumed to be harmonic, we are able to quantitatively reproduce coherent oscillations recently reported for this system [H. Uemura and H. Okamoto, Phys. Rev. Lett. **105**, 258302 (2010); T. Miyamoto, H. Uemura, and H. Okamoto, J. Phys. Soc. Jpn. **81**, 073703 (2012)]. We demonstrate that the microscopic model with parameters optimized for ground state properties of TTF-CA also applies to the coherent dynamics following photoexcitation. The modulation of the frequency of coherent molecular oscillations at the frequency of the lattice phonon emerges naturally as due to strong anharmonic coupling between the two harmonic vibrational degrees of freedom through coupling to delocalized electrons. Detailed comparison with experiment validates the model and sheds light on other aspects of photoinduced dynamics, including the almost instantaneous transfer of several electrons upon absorption of a single photon, as due to a cooperative effect of electronic correlations and molecular vibrations.

DOI: 10.1103/PhysRevB.91.174301 PACS number(s): 63.20.−e, 64.70.kt, 78.20.Bh, 78.47.−p

I. INTRODUCTION

Mixed-stack charge-transfer (MS-CT) crystals contain one-dimensional (1D) stacks of planar π-electron donors (D) and acceptors (A) arranged face-to-face as schematically shown in Fig. 1 [1,2]. CT between adjacent molecules leads to electron delocalization along the stack, a narrow bandwidth $4\tau < 1$ eV and fractional charges $\ldots D^{\rho+}A^{\rho-}D^{\rho+}A^{\rho-}\ldots$ with $0 < \rho < 1$. Weak D and A systems have $\rho \sim 0$, the strongest D and A reach $\rho \sim 1$, a few MS-CT crystals have $\rho \sim 0.5$, and fewer still have temperature/pressure dependent ρ as a result of a delicate balance between large competing electronic energies [3–5]. Among these rare MS-CT crystals, the first and most extensively studied [6–9] is TTF-CA, with D = tetrathiafulvalene (TTF) and A = Chloranil (CA) [Fig. 1(a)]. TTF-CA is an interesting system for exploring the physics of strong correlations in low dimensions and intrinsically soft lattices.

MS-CT crystals are currently investigated as promising all-organic ferroelectrics and have been suggested as potential multiferroics [10–13]. The rich phase diagram of MS-CT crystals provides opportunities to study quantum phase transitions [14], while multistability is the key to switchable materials and, more specifically, to switchable ferroelectrics [15]. A neutral-ionic phase transition (NIT) occurs in some MS-CT crystals on cooling or under pressure [3–6]. Lattice compression increases the electrostatic (Madelung) energy and drives the system from a neutral phase (N, $\rho < 0.5$) to an ionic phase (I, $\rho > 0.5$). MS-CT crystals are band insulators with conditional Peierls instability to dimerization in the limit of vanishing electron-electron interactions [16]. They are Mott insulators in the limit $\rho = 1$ with an unpaired electron at every site and antiferromagnetic Heisenberg exchange between neighbors. The spin chain is unconditionally unstable to dimerization in a spin-Peierls transition. The I phase of correlated models has a generalized Peierls instability to dimerization [16–18]. NIT physics is very rich: both continuous and discontinuous transitions are known [3,19] and cryogenic T_c has been reached [14]. Metastable phases are possible in systems with a discontinuous NIT [20] and are populated in photoinduced phase transitions [21–25], illustrating the physics of strongly correlated electronic systems coupled to both lattice phonons and molecular vibrations.

The phase diagram of MS-CT stacks and their ground state properties are well understood based on a minimal microscopic model, Eq. (1), below [20,26–28]. The electronic system is a half-filled Hubbard model with different site energy for D and A. Linear coupling to nuclear motions is introduced in the adiabatic (Born-Oppenheimer) approximation to two zone-center modes. The optical phonon for lattice dimerization modulates the hopping integrals τ (Peierls coupling) and a molecular vibration of either D or A modulates the site energies (Holstein coupling). The model has been solved via numerical diagonalization of finite 1D stacks using the valence bond (VB) basis and a mean-field approximation for 3D electrostatic interactions [20]. Satisfactory results have been obtained for such ground state properties of NIT systems as the ionicity ρ, lattice dimerization [20,27], polarization [29], dielectric constant [30], vibrational spectra [27,28], and diffuse x-ray scattering [31].

*anna.painelli@unipr.it

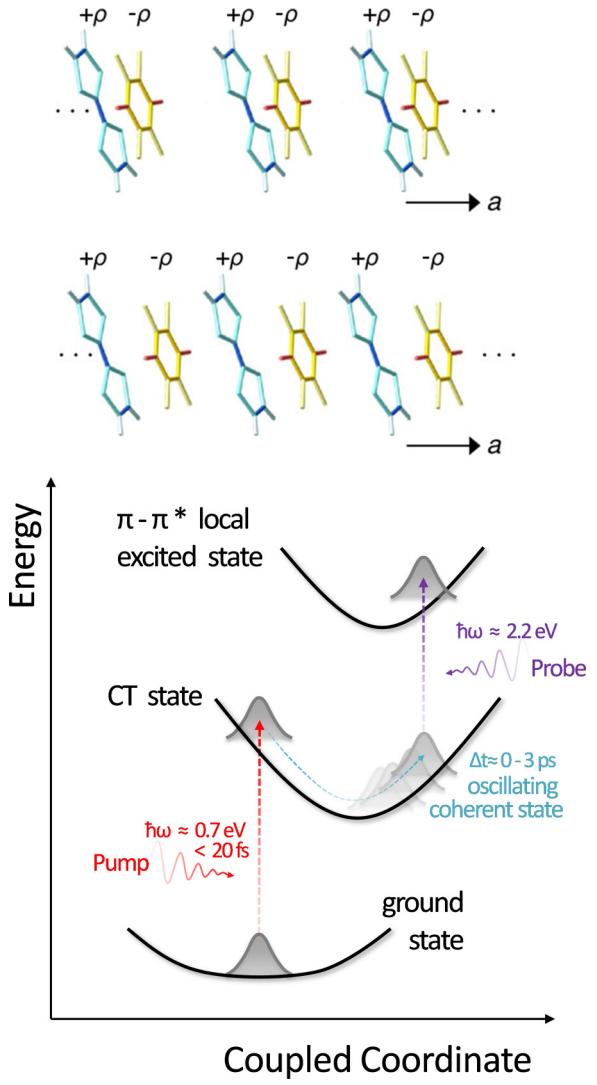

FIG. 1. (Color online) Top: a schematic view of a regular and a dimerized TTF-CA stack. Bottom: a pictorial view of the ultrafast pump and probe experiment.

The short-time dynamics following ultrafast photoexcitation of TTF-CA crystals have recently been reported by Okamoto and co-workers in a series of beautiful experiments [32,33]. Coherent oscillations are observed in pump-probe experiments with time resolution shorter than 20 fs. In this paper, we extend the microscopic NIT model to coherent oscillations at short times, $t \leqslant 3$ ps. A 1D model captures the initial dynamics, although photoinduced NIT and the long-time dynamics related to metastable states remain beyond the scope of 1D models.

Figure 1 shows a schematic view of the experiment [32,33]. The pump pulse of frequency ∼0.7 eV is polarized along the stack and generates CT excitations. Electron transfer is from D to A in neutral crystals at $T > T_c = 81$ K and from A to D in ionic crystals at $T < T_c$. The probe pulse is polarized perpendicular to the stack in the range of $\pi - \pi^*$ transitions. The photon energy of 2.25 eV is chosen at the maximum difference ΔR between the reflectance at $T = 77$ K on the ionic side and $T = 90$ K on the neutral side. Uemura and Okamoto [32] reported oscillating $\Delta R/R$ as a function of the delay time $\leqslant 3$ ps between pump and probe of a TTF-CA crystal at different temperatures from 90 to 260 K. Coherent oscillations are superimposed on a background at frequencies that closely match the frequencies of coupled vibrations observed in infrared or Raman spectra. The amplitude of the oscillation is large close to NIT ($T = 90$ K) and decreases upon increasing temperature [33]. Moreover, an anomalous behavior is observed for the low-frequency oscillation, the one associated with the lattice mode: at 90 K in fact the signal shows a rapid variation in the first 500 fs before oscillations start around a position different from the initial one. At high $T = 260$ K the rapid initial evolution is missing. Another interesting result comes from the wavelet analysis of the high frequency oscillations, related to molecular vibrations: the relevant frequency is modulated at the frequency of the lattice mode, suggesting a strong coupling between the two oscillations [32].

Here we extend the 1D model of MS-CT stacks to coherent oscillations at short times in systems close to and far from NIT. The paper is organized as follows. The microscopic model of MS-CT stacks in Sec. II has multiple phases close to the NIT, a stable N phase at T slightly higher than T_c, and degenerate metastable I phases. The molecular mode q and the lattice mode δ yield adiabatic potential energy surfaces (PES) for the ground state, $E_0(q,\delta)$, and lowest CT state, $E_1(q,\delta)$, that touch at a conical intersection. Diabatic PES [34] are constructed in Sec. III in order to model the evolution of vertical excitation in the N phase towards a metastable minimum of the I phase. Early time dynamics of $q(t)$ and $\delta(t)$ on diabatic PES are treated as classical motion with inverse friction constants taken as the experimental lifetimes [32,33]. The Fourier transforms (FT) of $q(t)$ and $\delta(t)$ give access to the frequencies of coherent oscillations and account naturally for the observed coupling of the two modes that enter the Hamiltonian as strictly harmonic and decoupled. Initial dynamics are modeled in Sec. IV for system at T well above T_c, far from NIT and multistability. We consider multielectron transfer in Sec. V, the possibility that CT absorption generates ionic domains as suggested on experimental grounds. We then briefly discuss the main results.

II. MICROSCOPIC MODEL FOR MS-CT STACKS

The following microscopic model is minimally needed to capture the physics of CT molecular crystals, dimers, and oligomers: (i) the electronic ground states (GS) energies of neutral molecules D, A and of their radical-ions D^+, A^-; (ii) the Mulliken CT integral $\tau = \langle D^+A^-|\mathcal{H}|DA\rangle$ for electron transfer and its linear dependence on intermolecular separation; (iii) coupling to a representative molecular vibration q, modulating on-site energies; and (iv) Coulomb interactions between ions [20,26–28,35]. The electronic and vibrational degrees of freedom can be treated explicitly in small molecular systems such as push-pull chromophores and related dyes [36–39]. Additional approximations are required in extended systems such as MS-CT crystals with 1D electron transfer and 3D Coulomb interactions.

The microscopic model of TTF-CA and related MS-CT crystals is defined by the following Hamiltonian [20,26–28]:

$$\mathcal{H} = (\Gamma + q)\sum_{p}(-1)^{p}\hat{n}_{p} - \tau\sum_{p,\sigma}[1+(-1)^{p}\delta](c^{\dagger}_{p,\sigma}c_{p+1,\sigma} + \text{H.c.}) + \sum_{p,q}^{3D} V_{pq}\hat{\rho}_{p}\hat{\rho}_{q} + N\frac{q^{2}}{2\epsilon_{v}} + N\frac{\delta^{2}}{2\epsilon_{d}}, \quad (1)$$

where p runs on the N sites and H.c. stands for Hermitian conjugate. The operators $c^{\dagger}_{p,\sigma}$ and $c_{p,\sigma}$ create and annihilate, respectively, an electron with spin σ on site p, and $\hat{n}_{p} = \sum_{\sigma} c^{\dagger}_{p,\sigma}c_{p,\sigma}$ counts the electrons on site p. The number operator is related to the charge on the A site (p even) as $\hat{\rho}_{p} = -\hat{n}_{p}$ and on the D site (p odd) as $\hat{\rho}_{p} = 2 - \hat{n}_{p}$. The average ionicity is calculated as $\rho = \langle \hat{n}_{p} \rangle$. 2Γ is the energy to create D^{+}, A^{-} at infinite separation. Doubly ionized sites, D^{2+} and A^{2-}, are excluded on physical grounds [16,20]. The electronic part of the above Hamiltonian represents the $U \to \infty$ limit of the modified Hubbard model (MHM) [40]. Only vibrational modes at the center of the Brillouin zone are accounted for: one lattice (Peierls) phonon, δ, modulating the dimerization amplitude and hence the hopping integrals, and one molecular vibration q modulating the on-site energy alternation Γ. The vibrational kinetic energy is disregarded in the adiabatic approximation. The vibrational coordinates δ and q are harmonic and are expressed in energy units, so that their coupling to the electronic system is fully defined by the parameters ϵ_{d} and ϵ_{v}, respectively [17,18,26].

Coulomb interactions V_{pq} run on all sites of the 3D crystal lattice and can be treated in two limits [20]: (i) a mean-field approximation reduces the problem to a 1D Hamiltonian with electrostatic interactions V between nearest neighbor and Madelung energy $E_{M} = \sum_{q}^{3D} V_{pq}$; (ii) a model with $E_{M} = 2V$ limited to nearest-neighbor interactions in Eq. (1) that are treated explicitly. The two approaches lead to qualitatively similar results. In the following we will mainly rely on (ii) and will point out where the choice of the approximation matters. In either case, we solve $\mathcal{H}$ in Eq. (1) exactly for 1D stacks up to 16 sites with periodic boundary conditions [41].

Plots of the GS energy, $E_{0}(q,\delta)$, have already been reported for TTF-CA parameters [20]. The relevant adiabatic potential energy surface (PES) evolves with increasing V that mimics lattice compression upon cooling or under applied pressure. We adopt standard parameters for TTF-CA, originally extracted from experiment [42] and recently validated by DFT [29], setting τ as the unit of energy and $\Gamma = 0.5$, $\epsilon_{d} = 0.28$, $\epsilon_{v} = 1.8$, and taking $\tau = 0.21$ eV when absolute energies are needed. Close to the NIT, a narrow range of V leads to a PES with three minima.

Figure 2 shows $E_{0}(q,\delta)$ as well as $E_{1}(q,\delta)$, the PES of the lowest singlet excited state, for $V = 1.55$ in the region of tristability. The absolute minimum corresponds to a regular stack with $q = q_{N}$, $\delta = 0$ in Fig. 2(b) and $\rho \sim 0.2$ in the N phase; the two metastable minima at $q = q_{I}$, $\delta = \pm\delta_{I}$ in Fig. 2(b) correspond to two equivalent dimerized stacks with

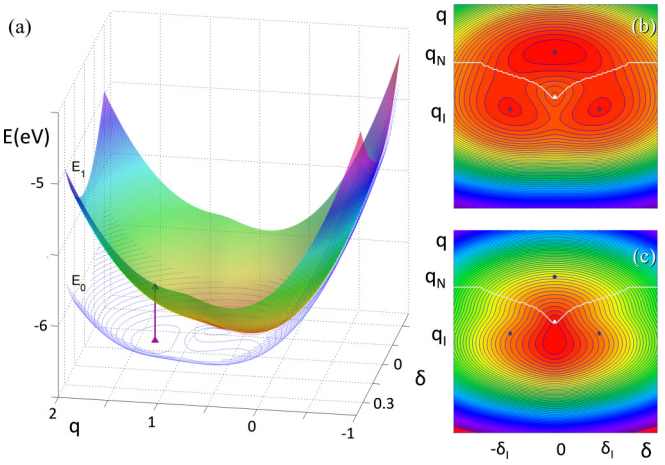

FIG. 2. (Color online) Ground and first excited state PES, calculated in the tristability region ($V = 1.55$). Main panel (a) shows the ground state PES as contour lines, and the first excited state as a color map. The arrow marks the vertical optical excitation. Panel (b) shows the color map and contour line for the ground state PES: the dots mark the stable state at $\delta = 0$, $q = q_{N}$, and the metastable states at $\delta = \pm\delta_{I}$, $q = q_{I}$. The white line is the line of minimum energy difference between the two PES that are degenerate at the conical intersection, shown as a white dot. Panel (c) shows the same information over the color map and contour plots relevant to the PES of the first singlet excited state. In all panels, q and δ coordinates are measured in units with $\tau = 1$.

$\rho \sim 0.6$ in the I phase. The excited state PES in Fig. 2(c) has a single minimum at $q = q_{E}$ and $\delta = 0$.

A short (<20 fs) excitation pulse with energy in the CT absorption region and polarized along the stack induces CT transitions from the GS. For $V = 1.55$ and TTF-CA parameters, we have calculated the first four excited states (up to an excitation energy of 0.7 eV). The corresponding oscillator strengths f_{j} were found using the dipole velocity operator, consistent with PBC [43]. The largest by an order of magnitude is f_{1} to the first excited state, corresponding to the transition shown with an arrow in Fig. 2(a). We therefore conclude that excitation is mainly to the $E_{1}(q,\delta)$ surface. The calculated transition energy of 0.36 eV is close to the observed maximum around 0.5 eV of the CT band of TTF-CA [32].

Finite-size calculations hardly capture the physics of phase transitions. In a first order transition, the GS of different phases are asymptotically decoupled. This decoupling cannot be achieved in finite systems. Indeed, the conical intersection between the GS and excited-state surfaces is the only indication of a discontinuous phase transition. The three minima of $E_{0}(q,\delta)$ correspond to the three phases of the infinite system. In this sense, the adiabatic approximation in Eq. (1) and the restriction to zone-center vibrations are more appropriate for quantum phases than for optical excitation.

The absorption of a single photon cannot induce a macroscopic phase transition but instead generates metastable excited domains in systems close to NIT as pointed out by Nagaosa [44]. Numerical simulation of excited 1D domains and domain walls are limited to uncorrelated Huckel or

spinless fermion systems of hundreds or thousands of sites [20]. We will approximate metastable domains in infinite 1D stacks by $E_1(q,\delta)$ in finite stacks with PBC. Photoexcitation transfers population from the ground to excited-state PES. The transferred population evolves on the excited-state surface, eventually reaching the metastable minimum. Relaxation to the GS surface is a competing mechanism that we do not model here. We consider below how photoexcitation to $E_1(q_N,\delta = 0)$ in Fig. 2 evolves in time to either $E_0(q_I,\delta_I)$ or $E_0(q_I, -\delta_I)$. To do so requires some manipulation of adiabatic PES obtained from the diagonalization to transform them into diabatic (and hence disconnected) PES that mimic stable and metastable domains.

III. DIABATIC PES AND DYNAMICS

The construction of diabatic PESs is physically motivated but arbitrary to some extent [34], in contrast to adiabatic PESs that follow rigorously from a chosen model. The adiabatic PES in Fig. 2(a) touch at the conical intersection, $(q_C,\delta = 0)$, and depend only marginally on system size. The energy gap $\Delta E = E_1(q,\delta) - E_0(q,\delta)$ is minimized along the line shown in Figs. 2(b) and 2(c), as well as along the line at $\delta = 0$ and $q \leqslant q_C$ between the two I-minima, that is fixed by symmetry. We seek to retain adiabatic PES as far as possible for diabatic surfaces that cross along lines that minimize ΔE. Our strategy is illustrated in Fig. 3 [45].

The diabatic surface that corresponds to the I-metastable state is constructed by connecting the excited state adiabatic PES in Fig. 2(c) with the ground state adiabatic PES in Fig. 2(b) along the lines where the energy gap between the two states is at a minimum (the white line in the two panels). The diabatic PES is $E_1(q,\delta)$ on the N side [the upper part of the q,δ plane in Figs. 2(b) and 2(c)] and $E_0(q,\delta)$ on the I side (the lower part of the q,δ plane). At $\delta = 0$ the adiabatic $E_1(q,\delta)$ and $E_0(q,\delta)$ surfaces cross and, as shown in Fig. 3(a), the diabatic PES does not require any adjustment. At finite δ some smoothing is needed, as exemplified in Fig. 3(b) for $\delta = 0.04$. We impose that along the sewing line the diabatic PES energy is the average of the two adiabatic energies; then we consider a small region around the sewing point where the diabatic PES is calculated as the weighed average of the adiabatic PES. Smoothing is limited to a narrow region close to the conical intersection. The width of the smoothing region increases away from the intersection. We choose the minimum width leading to a continuous diabatic PES with a continuous monotonic first derivative [45].

The diabatic PES corresponding to the metastable I-PES [whose sections at $\delta = 0$ and 0.04 are shown in Figs. 3(a) and 3(b)] has two equivalent minima at $\pm\delta_I$. We will evolve photoexcitation at $E_1(q_N,\delta = 0)$ along the smooth diabatic surface corresponding to the I-PES. Since the dynamics stays away from the sewing line, the details of the smoothing procedure are not important.

The procedure could be repeated to generate diabatic PES with a single minimum by cutting and sewing the ground and excited PES along the $\delta = 0$ line up to the conical intersection. However, the minima at $q_I, \pm\delta_I$ are close together and the diabatic surfaces obtained would significantly differ from the adiabatic PES in the region of the metastable minima.

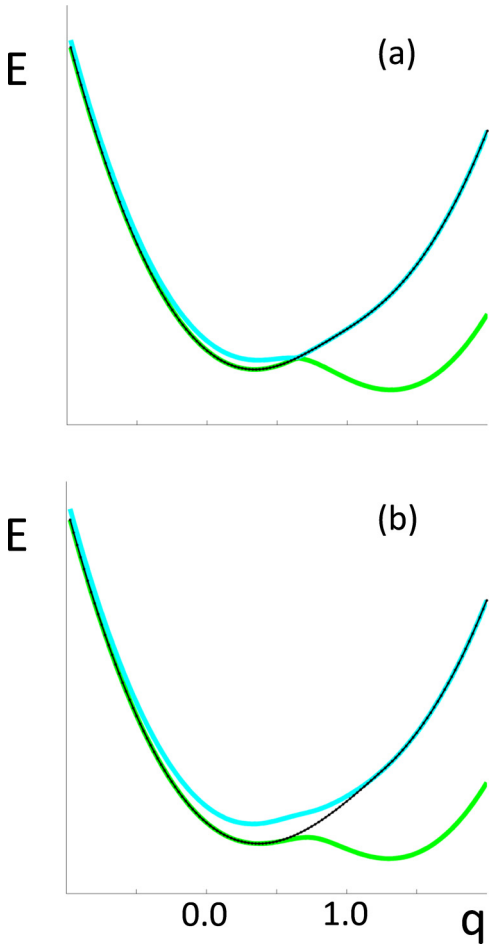

FIG. 3. (Color online) Construction of the metastable diabatic surface (black) from the adiabatic ground and first excited state (green and blue, respectively). Panels (a) and (b) refer to sections at $\delta = 0$ and $\delta = 0.04$. The adiabatic PES cross at $\delta = 0$. In all panels, E, q, and δ coordinates are measured in units with $\tau = 1$.

We therefore decided to use a single diabatic surface for the metastable I state showing two equivalent minima (see Figs. 4 and 5). In the following we will ensure that no trajectory of the photoexcited system crosses $\delta = 0$, thus effectively recovering the asymptotic decoupling of the two dimerized phases.

We are now in the position to address the dynamics following ultrafast excitation in the CT region of TTF-CA in the close proximity of the NIT ($T = 90$ K). After subtracting a large but featureless background that includes relaxation to the GS, the experimental $\Delta R/R$ signal in Ref. [32] shows coherent oscillations relevant to a lattice mode at 53 cm^{-1}, and four additional oscillations in the region of molecular vibrations at 320, 438, 740, and 957 cm^{-1}. The empirical analysis of Uemura and Okamoto describes each molecular oscillation as $A\cos(\omega t + \phi)\exp(-t/\tau)$ with adjustable amplitude A, frequency ω, phase ϕ, and lifetime τ (Table 1, Ref. [32]). The lattice mode requires two additional sets of A, ϕ, and τ parameters. Specifically, two contributions are assumed, one with a large A and a short $\tau = 0.19$ ps that accounts for an initial jump and a second contribution with small A and long $\tau = 5.25$ ps that damps the 53 cm^{-1} oscillation.

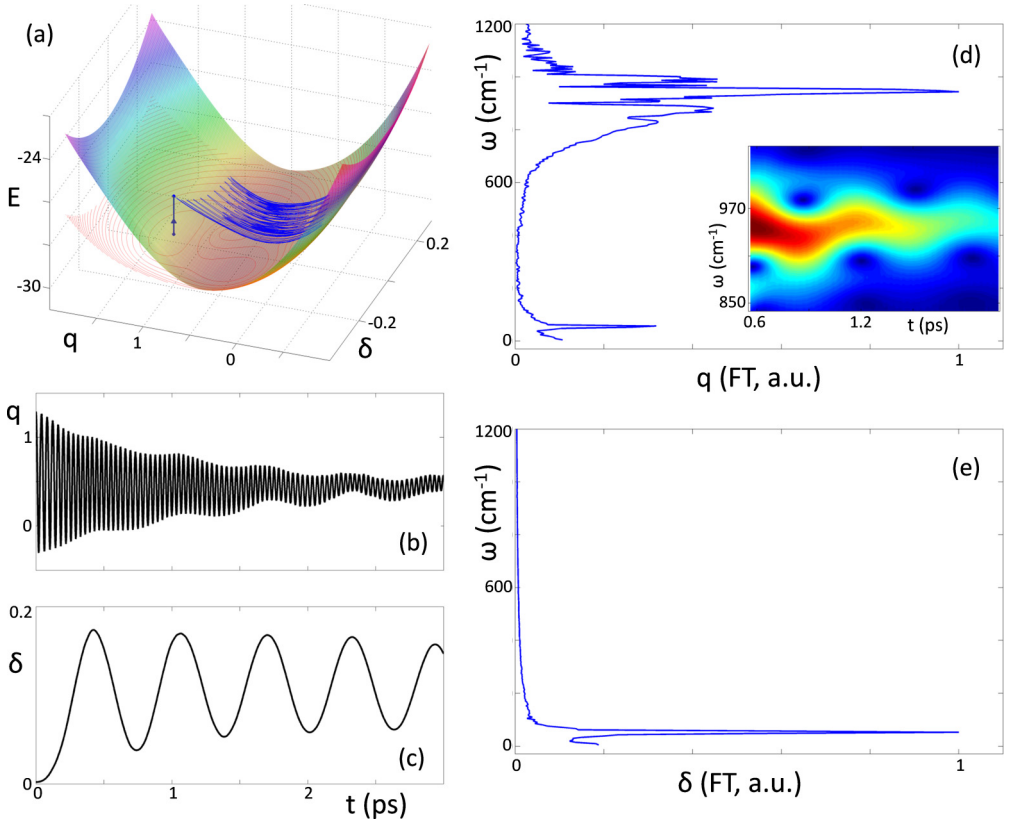

FIG. 4. (Color online) Classical dynamics over the diabatic PES: (a) a sketch of the dynamics following impulsive excitation; (b) calculated q vs time; (c) calculated δ vs time; (d) the normalized Fourier transform of $q(t)$ in panel (b), the inset shows the relevant spectrogram; (e) the normalized Fourier transform of $\delta(t)$ in panel (c). Energy and vibrational coordinates are measured in units with $\tau = 1$. Results are calculated for the single trajectory starting at $E_1(q_n,\delta = 0)$, as sketched in panel (a).

Vibrational spectra of TTF-CA in the molecular and lattice regions have been extensively studied. Indeed several lattice vibrations are coupled to the electrons through a Peierls mechanism, showing up as an effective Peierls mode with a frequency that softens from $\sim$70 cm^{-1} at 300 K (far from NIT) to 20 cm^{-1} at 90 K [46]. Coupled modes in the mid-IR region correspond to totally symmetric molecular vibrations of isolated TTF and CA species modulating on-site energies [Γ in Eq. (1)] [47]. Relevant frequencies and coupling constants were estimated long ago to simulate mid-IR and Raman vibrational spectra, associated with oscillations on the ground state PES [42,47]. To keep the picture as simple as possible while including all relevant interactions [20,28], we collapse all Peierls modes in a single lattice vibration, δ, and all molecular modes into a single effective mode, q, arbitrarily choosing to reproduce just the oscillation observed at 957 cm^{-1} in the molecular vibration region.

With this approximation, we can reproduce coherent oscillations of the ultrafast pump and probe signal, calculating the classical dynamics of the photoexcited system in the diabatic PES. The equilibrium system is described as a particle at the thermodynamically stable minimum, the N minimum at $(q_N,\delta = 0)$ of the ground state PES. Photoexcitation drives the system to the first excited state PES at $E_1(q_N,\delta = 0)$. Subsequent dynamics occurs on the diabatic I-PES, as schematically shown in Fig. 4(a). The system trajectory on the I-PES is calculated using the Verlet algorithm [48] to integrate the classical equations of motion:

$$\ddot{\delta} = -\frac{\epsilon_d}{N}\Omega_d^2\frac{\partial E}{\partial \delta} - \frac{\dot{\delta}}{\tau_d}, \tag{2}$$

$$\ddot{q} = -\frac{\epsilon_v}{N}\Omega_v^2\frac{\partial E}{\partial q} - \frac{\dot{\delta}}{\tau_v}, \tag{3}$$

where dots indicate time derivatives, Ω_d and Ω_v are the reference harmonic frequencies associated to δ and q oscillators [28], and τ_d and τ_v are the corresponding inverse friction coefficients. All electronic properties, including the adiabatic PES and the resulting diabatic PES, are fully defined by the model parameters entering the Hamiltonian in Eq. (1), and fixed in Sec. II according to previously published work. However, to calculate the real-time dynamics of the system, according to Eqs. (2) and (3), we must assign a mass to the coordinates, or, equivalently, a reference frequency [28]. These quantities are fixed as $\Omega_d = 66$ cm^{-1} and $\Omega_v = 1200$ cm^{-1} that best reproduce experimental data by Okamoto. Finally, the friction coefficients, $\tau_d = 5.25$ ps and $\tau_v = 0.65$ ps, are set to the experimental estimates from Okamoto [32]. Explicitly accounting for relaxation is important not just to recover the observed damping of coherent oscillations, but is instrumental in our calculation: energy dissipation (modeled by friction) drives the system towards one of the

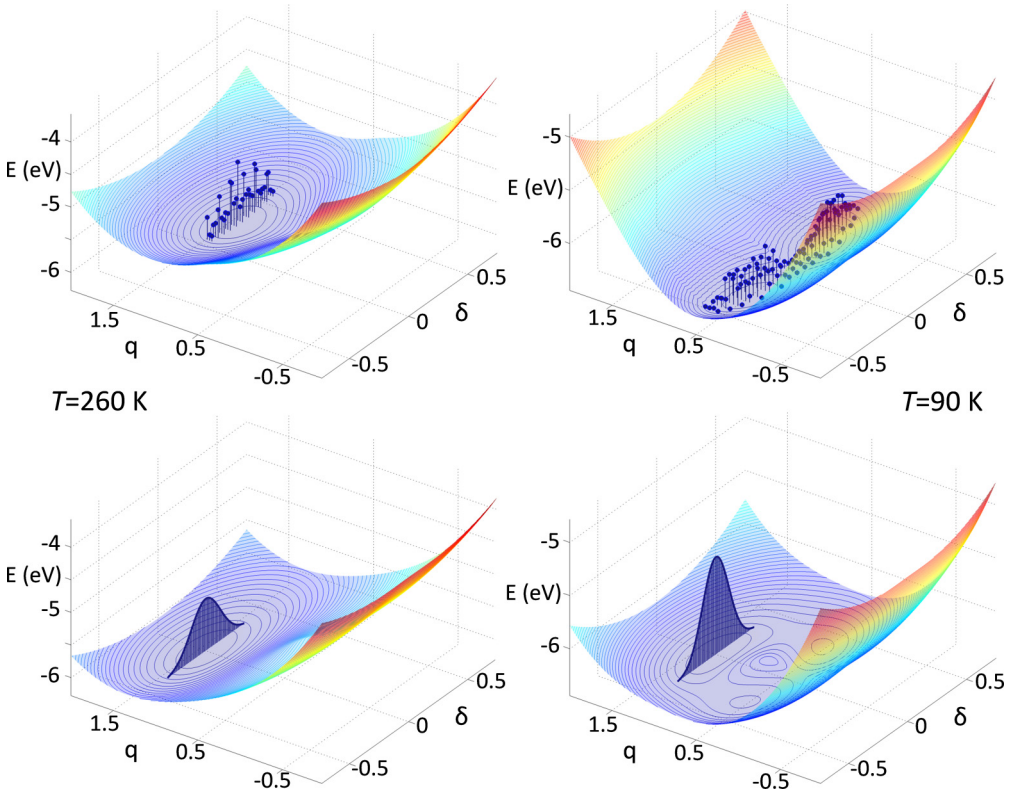

FIG. 5. (Color online) Sketch of the distributions in the (q,δ) plane (the distribution of p_δ momenta is not shown, but accounted for). Bottom panels show the initial Boltzmann distribution on the ground state PES; top panels show the distribution calculated after 3 ps evolution on the relevant PES, shown as color maps and contour plots. Left panels show results for $V = 1.2$ mimicking photoexcitation far from NIT on the N side. The bottom panel shows the ground state PES and the relevant equilibrium δ distribution ($T = 260$ K); the upper panel shows the excited state adiabatic PES and the distribution calculated after 3 ps evolution. The right panels refer to a system at NIT, with $V = 1.55$: the bottom panel shows the ground state PES and the relevant distribution; the upper panel shows the diabatic I-PES and the calculated distribution after 3 ps evolution. Vibrational coordinates are measured in units with $\tau = 1$.

two I-PES minima and avoids the switching between the two equivalent wells that would be otherwise possible in finite systems.

Figure 4(a) traces the motion of a system described by a single trajectory starting at $E_1(q_N,\delta = 0)$ in the I-PES surface. The time evolution $q(t)$ and $\delta(t)$ are shown in panels (b) and (c) up to 3 ps; friction damps the coherent oscillations. Fourier transforms (FT) of the two signals are shown in panels (d) and (e). The q and δ coordinates clearly oscillate at frequencies $\sim$945 and 55 cm^{-1}, respectively. These frequencies do not coincide with the reference frequencies because of the perturbations introduced by the coupling to electrons [47].

The calculated q oscillations in Fig. 4(b) follow directly from the dynamics on diabatic PES calculated based on a modified Hubbard model with ground state parameters. Vertical excitation at $t = 0$ in Fig. 2(a) from $E_0(q_N,\delta = 0)$ to $E_1(q_N,\delta = 0)$ implies a vanishing phase in the observed oscillations, $\phi = 0$. Moreover, the $q(t)$ trajectory starts at $q = q_N$, rapidly evolving towards q_I (the equilibrium q for the photoexcited I state), reaching $2q_I - q_N$ at $t = \pi/\omega_v$. Vertical excitation and fast $q(t)$ dynamics fully account for the observed initial rise of $\Delta R/R$ without the need to postulate an additional oscillation with $\tau = 0.19$ ps [32]. After the initial increase, $q(t)$ oscillates about q_I with an amplitude $q_I - q_N$ that progressively decreases due to friction.

The frequency ω_v is slightly lower that the reference frequency Ω_v in Eq. (4) and is modulated by the δ oscillations as seen in Fig. 4(d). This modulation is not introduced *ad hoc* in the model, but follows naturally from the large anharmonicity of the PES and can be easily understood. In fact, since $\omega_v > 10\omega_d$, one can separate the q and δ motion adopting a sort of adiabatic approximation for δ. Accordingly, $q(t)$ in Eq. (3) becomes $q(t;\delta)$ and its frequency ω_v acquires a δ dependence, resulting in a ω_d modulation of $\omega_v(\delta)$. In other terms, while δ oscillates, different regions of the PES are explored, that, due to the large anharmonicity, are characterized by a different curvature along the q coordinate.

The microscopic model, Eq. (1), with adiabatic PES and vertical excitation immediately simulates the observed coherent vibrations with a minimum number of parameters. Specifically, the q and δ oscillations and their FT agree quantitatively with the experimental results in Ref. [32], an impressive result since we are using the previous model for TTF-CA with ground state parameters. The only new or readjusted parameters are the two reference frequencies, $\Omega_d = 66$ cm^{-1} and $\Omega_v = 1200$ cm^{-1}, chosen to reproduce the frequency of the Peierls mode and of one molecular vibration. The other parameters in this work are the friction coefficients taken as the experimental inverse relaxation times. By contrast, the empirical fit in Ref. [32] has seven parameters for the

low-frequency oscillation of $\delta(t)$ and four parameters for each of the molecular oscillations $q(t)$. The observed complex phenomenology is due to highly anharmonic PES near the NIT and is quantitatively captured by the modified Hubbard model with linear coupling of delocalized electrons to molecular and lattice vibrations.

IV. PHOTOINDUCED DYNAMICS FAR FROM NIT, AND THE ROLE OF TEMPERATURE

Coherent oscillations measured in Ref. [33] for TTF-CA at $T > T_c$, up to 260 K, pose additional challenges to the microscopic model, as well as additional constraints. The system is now far from the NIT and multistability. To model high-T data, we decrease V in Eq. (1) from $V = 1.55$ for 90 K in the tristability region to $V = 1.2$, where the system is safely in the N side. The adiabatic PES of $E_0(q,\delta)$ and $E_1(q,\delta)$ in Fig. 5, left panels, have a single minimum, both at $\delta = 0$, and no conical intersection. In the absence of metastable states, light absorption cannot induce a phase transition. Absorption of a photon generates a CT excitation whose dynamics may be treated using adiabatic PES. As noted above, we restricted Eq. (1) to molecular and lattice vibrations at the zone center, $k = 0$, in order to make the extended correlated model tractable. A direct consequence of $k = 0$ vibrations is that every electronic state has identical q and δ at all sites, thereby excluding local relaxation along either coordinate. Different electronic states of finite systems may of course have different q, as illustrated in Fig. 5.

Vertical excitation of a classical particle from $E_0(q_N,\delta = 0)$ to $E_1(q_N,\delta = 0)$ only generates oscillations along q, while $\delta = 0$ stays fixed at equilibrium. An analysis similar to that in Sec. III would not reproduce the experimental data with oscillations of both q and δ, albeit with greatly reduced amplitude of δ oscillations compared to 90 K. To rationalize the experimental findings and to better understand low-T data as well, we refine our treatment to include thermal disorder.

Specifically, neglecting the minor thermal disorder associated with the high-frequency mode ($\hbar\Omega_v \gg kT$), we consider a thermal (Boltzmann) distribution of δ and its conjugate momentum, p_δ. The (δ, p_δ) plane is uniformly sampled in a regular 70×70 array of points, defining 4900 classical trajectories with different initial conditions, shown in Fig. 5.

Each trajectory is independently propagated the same way as in the previous section, and time-dependent properties are obtained by averaging over all trajectories. The FT of $\delta(t)$ and $q(t)$ are calculated for each trajectory and then combined, taking relative probabilities into account, to calculate the overall FT. While results at NIT are well understood even without accounting for thermal disorder, as discussed in Sec. III, for the sake of comparison Fig. 6 explicitly shows FT of δ and q signals calculated near the NIT and far from it

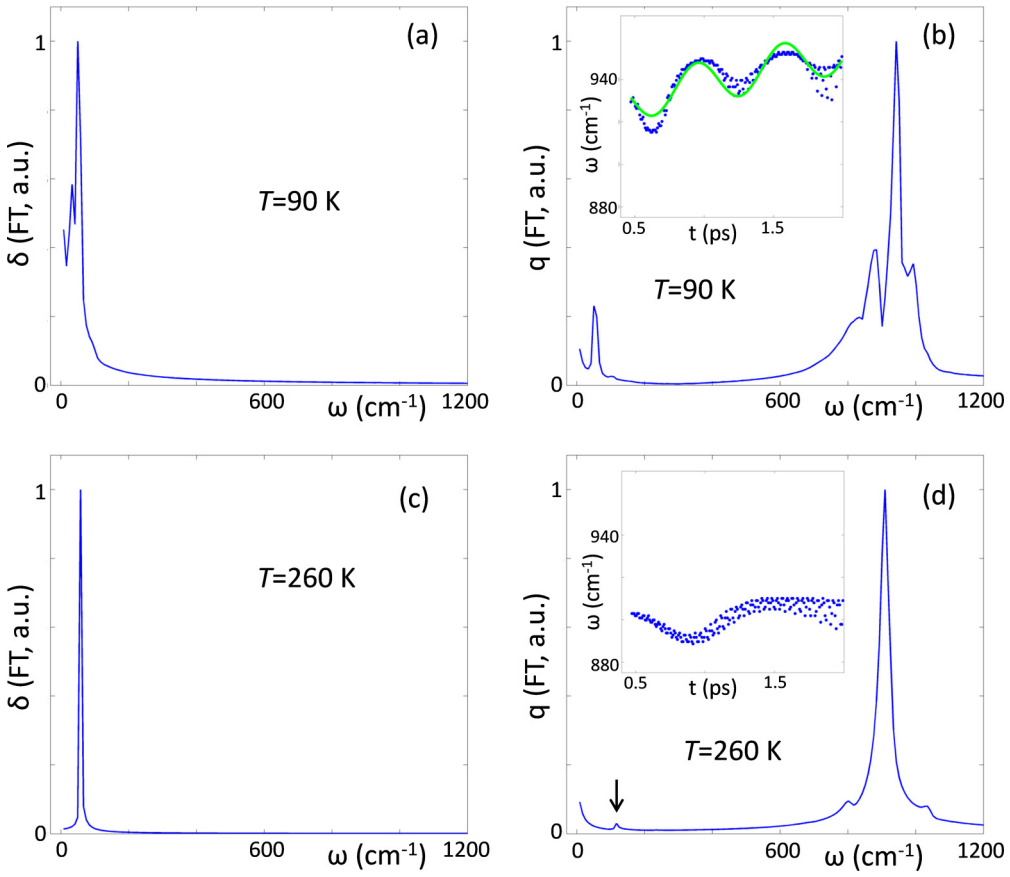

FIG. 6. (Color online) Normalized Fourier transform of the $\delta(t)$ and $q(t)$ signals (left and right panels, respectively) calculated accounting for the thermal distribution of δ and relevant momenta (see Fig. 5), for a system close to NIT ($V = 1.55$, $T = 90$ K, upper panels) and in the N regime ($V = 1.2$, $T = 260$ K, bottom panels). The insets in the right panels show the wavelet analysis of $q(t)$. The green curve in the inset to panel (b) is a fit to the wavelet signal, corresponding to a frequency of 54 cm^{-1}. Vibrational coordinates are measured in units with $\tau = 1$.

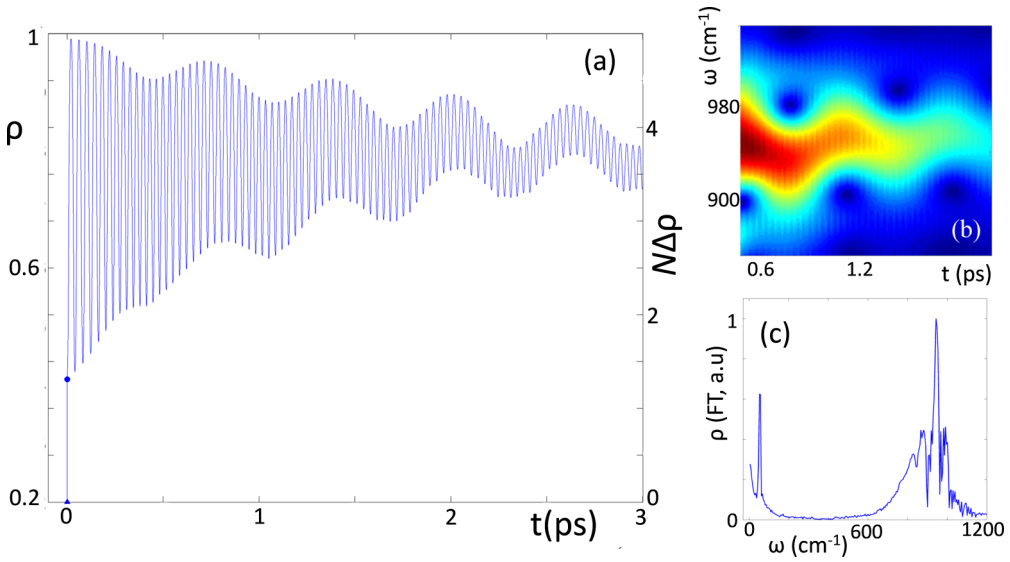

FIG. 7. (Color online) Main panel (a): the temporal evolution of ρ for the system described in Fig. 4. At $t = 0$ the triangle marks the ground state ionicity, ρ_N, and the dot marks the ionicity on the excited state upon vertical excitation, ρ_E. Panels (b) and (c) show the wavelet analysis and the normalized Fourier transform of $\rho(t)$ in panel (a).

for systems where thermal disorder is explicitly accounted for. Disorder hardly changes results at the NIT; the main difference is a small softening of calculated frequencies.

More interesting (and puzzling) are the results obtained at high T. The FT of δ has a 58 cm^{-1} peak at slightly higher frequency than calculated at NIT. The q-FT shows a high frequency peak at 908 cm^{-1}, slightly softer than at 90 K. However, q oscillations are modulated at twice the δ frequency, with the relevant FT clearly showing a 100 cm^{-1} peak, in sharp contrast with what happens at NIT, where the low-frequency peak in the q-FT occurs exactly at the same frequency as δ oscillations.

This result can be rationalized based on the qualitatively different shape of PES near the NIT or far from it. After vertical photoexcitation at 90 K, the system evolves from $\delta = 0$ towards one of the two minima at $\pm\delta_I$. Oscillations about the minimum modulate q, driving the systems in regions with slightly different curvature (anharmonicity). As a result, the frequency of q is modulated at the frequency of δ oscillations. Far from NIT, the photoexcited system oscillates around the equilibrium position, $\delta = 0$. As before, these oscillations modulate the frequency of the molecular vibration. Since many system properties, including the curvature of the PES, are symmetric around $\delta = 0$, the corresponding modulation is observed at twice the frequency of δ oscillations. Experimental data collected at high temperature [33] were not analyzed to show this frequency modulation. Our theoretical results suggest that a wavelet analysis of coherent excitation offers a reliable way to discriminate sharply between systems near NIT, where long-lived (metastable) photoexcited states are accessible, and systems far from NIT, where metastable states are not accessible.

V. MULTIELECTRON TRANSFER

We are now in the position to discuss how photoexcitation and the subsequent dynamics affect the ionicity ρ of excited domains. According to the adiabatic approximation for Eq. (1), the PES completely specifies $\rho(q,\delta)$. Figure 7(a) shows the evolution of $\rho(t)$ for the classical dynamics described in Sec. III; panels (b) and (c) show the corresponding FT and spectrogram. The first observation is that the results closely resemble those reported in Fig. 4 for the q coordinate. Indeed, at equilibrium the Hellmann-Feynman theorem applied to Eq. (1) leads to a direct proportionality between q and ρ:

$$q = \epsilon_v(1 - \rho), \tag{4}$$

so that oscillations of q and ρ are expected to be very similar. Much as q, the FT of $\rho(t)$ shows two peaks at 52 and 943 cm^{-1}, corresponding to the frequency of the Peierls and of the molecular mode. As before, the high frequency is modulated by the frequency of δ oscillations through the coupling to the electronic system. Indeed the spectrogram in Fig. 7(b) closely resembles the wavelet analysis of the experimental $\Delta R/R$ in Fig. 2(a) of Ref. [32].

The analysis of the $\rho(t)$ signal can help us shed light on the intriguing phenomenon of multielectron transfer. It has long been recognized that absorption of a single photon in MS-CT stacks may generate CT strings $(D^+A^-)_n$ with $n > 1$ [49–51]. The experimental estimate for TTF-CA is $n \sim 10$ within 20 fs [32]. Even larger n has been suggested within short times that are set by the experimental time resolution. A single photon generates extensive electronic motion that, as discussed elsewhere [49–51], is not expected in either one-electron molecular-orbital treatments or in exciton theories of molecular crystals or aggregates. Multielectron transfer is possible in 1D models with strong electronic correlations and carefully tuned parameters [49–51]. The microscopic model for MS-CT stacks in Eq. (1) has electronic and vibrational parameters that account for the ground state properties of TTF-CA and, as shown above, also for coherent oscillations. It is natural to ask what the model says about multielectron transfer.

The left y axis of Fig. 7(a) shows $N\Delta\rho(t) = N(\rho(t) - \rho_G)$, where ρ_G is the ground state ionicity at equilibrium. $N\Delta\rho(t)$ directly measures the total number of electrons transferred from D to A sites. The first important result is that the vertical excitation at $t = 0$ by itself transfers almost 1.5 electrons, clearly more than one. Transferring more than one electron upon absorption of a single photon is made possible by the correlation of the motion of electrons in the different cells [49]. To confirm the role of correlations, we repeated the calculation with a full mean-field approximation for Coulomb interactions in Eq. (1). Vertical excitation definitely transfers less than one electron when the potential at each cell is the average potential of the surrounding cells.

What is more interesting, however, is the role of molecular vibrations. Holstein coupling, that together with Madelung energy drives the discontinuous NIT [18,20], also contributes to multielectron transfer. As clearly shown the top left panel of Fig. 7, while vertical photoexcitation transfers just 1.5 electrons, about 4.8 electrons are transferred in less than 17 fs, the first half-period of the q oscillation, to stabilize towards 3.7 transferred electrons in the long time (3 ps) regime. This intriguing result is in semiquantitative agreement with the observation that photoexcitation generates a domain $(D^+A^-)_n$ with $n \sim 10$ within 20 fs.

The analysis of $\rho(t)$ upon photoexcitation at high T, far from NIT, does not add much to the discussion. Indeed, the correlation between electrons on different cells is reduced far from NIT, and the number of electrons transferred upon vertical photoexcitation $N\Delta\rho(0)$ is only marginally larger than 1 at $T = 260$ K. Moreover, much as with q, the FT of $\rho(t)$ calculated at NIT shows a peak at the frequencies corresponding to the q and δ oscillations, while the FT of the $\rho(t)$ signal calculated at 260 K shows two peaks, one at the frequency of q, the other at twice the frequency of δ oscillations.

VI. CONCLUSIONS

NIT is a prototypical example of a phase transition driven by correlated electrons in reduced dimensions that involves lattice relaxation and symmetry breaking. Continuous and discontinuous NIT have been studied extensively offering clues about strongly anharmonic lattice dynamics with important spectroscopic effects in vibrational spectra [28] and anomalous diffuse x-ray scattering peaks [31]. A comparatively simple model, that describes electrons in terms of a modified Hubbard Hamiltonian, and accounts for their coupling with (zone-center) lattice modes and molecular vibrations, has been successfully used and reliably parametrized to describe the rich physics of NIT. Multistability at discontinuous NIT offers the possibility to populate metastable states upon photoexcitation and photoinduced NIT have been studied in the past 20 years or so.

Modeling photoinduced transitions represents an enormous challenge. The settling of the system into a true metastable phase involves a complex interplay of all interactions, including 3D ordering, a difficult and very delicate issue to be modeled in strongly correlated electron systems, where only small clusters can be treated numerically. Moreover, finite-size effects are particularly prominent close to phase transitions, and must be properly taken into account.

Ultrafast photoexcitation induces coherent motion in excited state PES, that allows following the initial dynamics of the system and gives detailed information about the coupling between electronic and nuclear degrees of freedom in strongly anharmonic potentials. This elegant pump-probe experiment offers a unique opportunity to model photoexcitation: the observed dynamics in fact occur long before the locking in of 3D order. At 4 and 77 K, photoinduced transition is from I to N and has been followed on longer times. Metastable states populated at 77 K do not decay within the 500 ps of observation time supporting a true photoinduced phase transition [24]. By contrast, photoexcited states generated at 90 K decay much faster ($\sim$20 ps), even if hints of long-lived ($>$2000 ps) structural deformations are obtained from time-resolved x-ray diffraction studies [52]. In any case, in this work we focus on the first 3 ps following ultrafast excitation: a temporal window far too short to address the formation of truly metastable domains or their 3D locking as required for photoinduced NIT.

We have shown that the microscopic model for NIT (specifically for TTF-CA) also holds for the early stage dynamics following ultrafast photoexcitation. Finite-size effects at the phase transitions leading to a fictitious mixing of states corresponding to the three stable phases are overcome by resorting to diabatic states, whose PES are constructed based on the adiabatic PES calculated on finite clusters. The model quite naturally explains most experimental observations, in terms of the dynamics on metastable PES whose large anharmonicity leads to a coupling of molecular vibrations and lattice modes, that shows up with the modulation of the frequency of the molecular mode by the lattice mode.

The same model can also be adopted to study the dynamics following photoexcitation far from NIT. In this case light absorption drives the system to an excited state, not a metastable state. Coherent oscillations are still seen with clear (even if less prominent) signatures of anharmonicity. Two major differences are however observed. At the phase transition the metastable state is a symmetry-broken (dimerized) state: the δ coordinate starts at zero but the system quickly relaxes towards the equilibrium relevant to the symmetry-broken state. By contrast, far from the phase transition the populated excited state stays undimerized and δ oscillates around the equilibrium. Our model nicely confirms experimental data in this respect. The second (more subtle) difference concerns the coupling between molecular and lattice vibrations and is again related to symmetry breaking. The δ oscillations about δ_I of the metastable state lead (due to anharmonicity) to a modulation of the frequency of the molecular vibration occurring at the frequency of δ oscillations. However, far from NIT δ oscillates about zero and, since the PES is symmetric with respect to δ, the modulation of the molecular frequency occurs at twice the frequency of the δ oscillations. This qualitative difference offers an opportunity to discriminate between systems with accessible metastable states where a photoinduced phase transition may be possible in principle, and systems where photoexcitation leads to short-lived excited states.

Our analysis also sheds light on the nature of photoexcited state: discontinuous NIT are driven by electrostatic interactions and Holstein coupling. Both interactions are responsible for a large entanglement of states with different number of

excitations generating almost unique properties. In particular we are able to demonstrate that, using our model with realistic parameters, at NIT the absorption of a single photon in a neutral lattice generates $\sim$10 D^+A^- pair in less than 20 fs.

ACKNOWLEDGMENT

Work in Parma supported by the Italian Ministry of Research and Education (MIUR) through Grant No. PRIN-2012T9XHH7.

[1] Z. Soos and D. Klein, in *Treatise on Solid-State Chemistry*, edited by N. B. Hannay (Plenum Press, New York, 1976), Vol. III, p. 689.
[2] Z. G. Soos, Annu. Rev. Phys. Chem. **25**, 121 (1974).
[3] A. Girlando, A. Painelli, S. A. Bewick, and Z. G. Soos, Synth. Met. **141**, 129 (2004), and references therein.
[4] S. Horiuchi, T. Hasegawa, and Y. Tokura, J. Phys. Soc. Jpn. **75**, 051016 (2006), and references therein.
[5] S. Horiuchi, R. Kumai, Y. Okimoto, and Y. Tokura, Chem. Phys. **325**, 78 (2006), and references therein.
[6] A. Girlando, R. Bozio, C. Pecile, and J. B. Torrance, Phys. Rev. B **26**, 2306 (1982).
[7] A. Girlando, F. Marzola, C. Pecile, and J. B. Torrance, J. Chem. Phys. **79**, 1075 (1983).
[8] M. Buron-LeCointe, M. H. Lemée-Cailleau, H. Cailleau, B. Toudic, A. Moreac, F. Moussa, C. Ayache, and N. Karl, Phys. Rev. B **68**, 064103 (2003).
[9] M. H. Lemée-Cailleau, M. LeCointe, H. Cailleau, T. Luty, F. Moussa, J. Roos, D. Brinkmann, B. Toudic, C. Ayache, and N. Karl, Phys. Rev. Lett. **79**, 1690 (1997).
[10] S. Horiuchi and Y. Tokura, Nat. Mater. **7**, 357 (2008).
[11] F. Kagawa, S. Horiuchi, H. Matsui, R. Kumai, Y. Onose, T. Hasegawa, and Y. Tokura, Phys. Rev. Lett. **104**, 227602 (2010).
[12] F. Kagawa, S. Horiuchi, M. Tokunaga, J. Fujioka, and Y. Tokura, Nat. Phys. **6**, 169 (2010).
[13] K. Kobayashi, S. Horiuchi, R. Kumai, F. Kagawa, Y. Murakami, and Y. Tokura, Phys. Rev. Lett. **108**, 237601 (2012).
[14] S. Horiuchi, Y. Okimoto, R. Kumai, and Y. Tokura, Science **299**, 229 (2003).
[15] T. Miyamoto, H. Yada, H. Yamakawa, and H. Okamoto, Nat. Commun. **4**, 2586 (2013).
[16] Y. Anusooya-Pati, Z. G. Soos, and A. Painelli, Phys. Rev. B **63**, 205118 (2001).
[17] A. Girlando and A. Painelli, Phys. Rev. B **34**, 2131 (1986).
[18] A. Painelli and A. Girlando, Phys. Rev. B **37**, 5748 (1988).
[19] P. Ranzieri, M. Masino, A. Girlando, and M.-H. Lemée-Cailleau, Phys. Rev. B **76**, 134115 (2007).
[20] Z. G. Soos and A. Painelli, Phys. Rev. B **75**, 155119 (2007).
[21] T. Suzuki, T. Sakamaki, K. Tanimura, S. Koshihara, and Y. Tokura, Phys. Rev. B **60**, 6191 (1999).
[22] T. Luty, H. Cailleau, S. Koshihara, E. Collet, M. Takesada, M. H. Lemée-Cailleau, M. B.-L. Cointe, N. Nagaosa, Y. Tokura, E. Zienkiewicz, and B. Ouladdiaf, Europhys. Lett. **59**, 619 (2002).
[23] E. Collet, M.-H. Lemée-Cailleau, M. B.-L. Cointe, H. Cailleau, M. Wulff, T. Luty, S.-Y. Koshihara, M. Meyer, L. Toupet, P. Rabiller, and S. Techert, Science **300**, 612 (2003).
[24] H. Okamoto, Y. Ishige, S. Tanaka, H. Kishida, S. Iwai, and Y. Tokura, Phys. Rev. B **70**, 165202 (2004).
[25] S. Iwai, Y. Ishige, S. Tanaka, Y. Okimoto, Y. Tokura, and H. Okamoto, Phys. Rev. Lett. **96**, 057403 (2006).
[26] A. Painelli, L. D. Freo, and Z. G. Soos, Synth. Met. **133–134**, 619 (2003).
[27] L. DelFreo, A. Painelli, and Z. G. Soos, Phys. Rev. Lett. **89**, 027402 (2002).
[28] G. D'Avino, M. Masino, A. Girlando, and A. Painelli, Phys. Rev. B **83**, 161105 (2011).
[29] G. D'Avino and M. J. Verstraete, Phys. Rev. Lett. **113**, 237602 (2014).
[30] Z. G. Soos, S. A. Bewick, A. Peri, and A. Painelli, J. Chem. Phys. **120**, 6712 (2004).
[31] G. D'Avino, A. Girlando, A. Painelli, M.-H. L. Cailleau, and Z. G. Soos, Phys. Rev. Lett. **99**, 156407 (2007).
[32] H. Uemura and H. Okamoto, Phys. Rev. Lett. **105**, 258302 (2010).
[33] T. Miyamoto, H. Uemura, and H. Okamoto, J. Phys. Soc. Jpn. **81**, 073703 (2012).
[34] T. V. Voorhis, T. Kowalczyk, B. Kaduk, L.-P. Wang, C.-L. Cheng, and QinWu, Annu. Rev. Phys. Chem. **61**, 149 (2010).
[35] K. Yonemitsu, J. Phys. Soc. Jpn **80**, 084707 (2011).
[36] L. Grisanti, G. D. Avino, A. Painelli, J. Guasch, I. Ratera, and J. Veciana, J. Phys. Chem. B **113**, 4718 (2009).
[37] F. Terenziani, A. Painelli, C. Katan, M. Charlot, and M. Blanchard-Desce, J. Am. Chem. Soc. **128**, 15742 (2006).
[38] C. Sissa, P. M. Jahani, Z. G. Soos, and A. Painelli, ChemPhysChem **13**, 2795 (2012).
[39] F. Terenziani, C. Sissa, and A. Painelli, J. Phys. Chem. B **112**, 5079 (2008).
[40] R. Resta and S. Sorella, Phys. Rev. Lett. **82**, 370 (1999).
[41] Z. G. Soos and S. Ramasesha, in *Valence Bond Theory and Chemical Structure*, edited by D. J. Klein and N. Trinajstic (Elsevier, New York, 1990).
[42] A. Painelli and A. Girlando, J. Chem. Phys. **87**, 1705 (1987).
[43] A. Painelli and Z. G. Soos, Chem. Phys. **325**, 48 (2006).
[44] N. Nagaosa, J. Phys. Soc. Jpn. **55**, 3488 (1986).
[45] L. Cavatorta, Master degree thesis, Dipartimento di Chimica, Università di Parma, 2013.
[46] A. Girlando, M. Masino, A. Painelli, N. Drichko, M. Dressel, A. Brillante, R. G. D. Valle, and E. Venuti, Phys. Rev. B **78**, 045103 (2008).
[47] A. Painelli and A. Girlando, J. Chem. Phys. **84**, 5655 (1986).
[48] L. Verlet, Phys. Rev. **159**, 98 (1967).
[49] A. Painelli and F. Terenziani, J. Am. Chem. Soc. **125**, 5624 (2003).
[50] F. Terenziani and A. Painelli, Phys. Rev. B **68**, 165405 (2003).
[51] A. Painelli, F. Terenziani, and Z. G. Soos, Theor. Chem. Acc. **117**, 915 (2007).
[52] E. Collet, M. B.-L. Cointe, and H. Cailleau, J. Phys. Soc. Jpn. **75**, 011002 (2006).